Available online at www.sciencedirect.com
ScienceDirect
Acta Materialia 59 (2011) 6246–6256
Acta MATERIALIA
www.elsevier.com/locate/actamat

Thermodynamic modeling and experimental investigation of the phase stability at the Ni-rich region of the Ni–Al–Cr–Ir system

C. Zhang [a,*], F. Zhang [a], S.-L. Chen [a], W.-S. Cao [a], Y.A. Chang [a,b]

[a] CompuTherm LLC, 437 S. Yellowstone Dr., Suite 217, Madison, WI 53719, USA
[b] Department of Materials Science and Engineering, University of Wisconsin–Madison, 1509 University Avenue, Madison, WI 53706, USA

Received 10 May 2011; received in revised form 10 June 2011; accepted 18 June 2011
Available online 23 July 2011

Abstract

The effect of adding 3 at.% Cr on the phase stability of the Ni–Al–Ir system was studied experimentally at 1250 °C. A thermodynamic description of the Ni–Al–Cr–Ir quaternary system in the Ni-rich region was then developed based on the microstructures, the crystal structures and the phase compositions determined by experiment for eight alloys in both as-cast and 1250 °C annealed states. The calculated isothermal section at 1250 °C using the obtained description was consistent with the phase-equilibrium data obtained in this study. The calculated two-dimensional section of liquidus projection was also in accordance with the primary phases of solidification observed from alloys in the as-cast state. The effects of Cr additions to the Ni–Al–Ir alloys on the as-cast and annealed microstructures were elucidated through Scheil simulation and phase-equilibrium calculation using Pandat.

Keywords: Nickel alloys; Solidification microstructure; Annealing; Thermodynamics; CALPHAD

1. Introduction

Nickel-based superalloys are the most widely used high-temperature materials in gas turbine engines due to their superior resistance to creep, oxidation and fatigue at elevated temperatures. The major alloying elements in the current Ni-based superalloys are Al, Co, Cr, Mo, Ti, etc. [1]. In spite of the very complicated alloy compositions of commercial superalloys, the Ni–Al–Cr system provides the basis for most Ni-based superalloys. Recent interest in developing oxidation-resistant Ni-based superalloys in the forms of foils and thin sheets for high-temperature applications without coatings has motivated investigation of the phase stability of Ni-based superalloys containing metals of the platinum family, such as Pt and Ir [2–4]. Addition of Ir is known to improve the creep resistance and oxidation resistance of existing Ni-based superalloys. Further improvement, especially of intermetallic-based superalloys, calls for a better understanding of the thermodynamics and phase equilibria of the Ni–Al–Cr–Ir–M systems (where M represents all the other key components of Ni-based superalloys).

The objective of the present work is to study the effects of Cr addition on the phase stability and phase relationship in Ni–Al–Ir superalloys and obtain a thermodynamic description of the quaternary Ni–Al–Cr–Ir system using the computational/experimental approach, which has been shown to be a highly efficient method for thermodynamic database development [5,6]. First, a preliminary thermodynamic description of the Ni–Al–Cr–Ir system was obtained on the basis of those of the constituent binary and ternary phases. Next, key alloys were selected for experimental investigation based on the calculated phase diagrams using the preliminary description. The experimental data obtained were then used to optimize the model parameters to obtain an improved thermodynamic description for this quaternary system. To develop a preliminary thermodynamic description of the Ni–Al–Cr–Ir system, we need to have thermodynamic descriptions of the following

* Corresponding author. Tel.: +1 608 395 1145.
E-mail address: czhang.wisc@gmail.com (C. Zhang).

1359-6454/$36.00
doi:10.1016/j.actamat.2011.06.034

lower-order systems: four unary systems; six binary systems (Ni–Al [7], Ni–Cr [8], Ni–Ir [9], Al–Cr [8], Al–Ir [10] and Cr–Ir [11]); and four ternary systems (Ni–Al–Cr [8], Ni–Al–Ir [9], Ni–Cr–Ir and Al–Cr–Ir). The descriptions of the Ni–Cr–Ir and Al–Cr–Ir systems are obtained from those of the constituent binary systems by extrapolation [12]. The preliminary thermodynamic description of the Ni–Al–Cr–Ir quaternary system was then developed from those of constituent ternary systems via extrapolation. In the following section, we will describe in detail the thermodynamic models used in this study.

2. Thermodynamic modeling

The following phases were considered at the Ni-rich region in the Ni–Al–Cr–Ir system: liquid, β ($B2$), ordered γ' ($L1_2$) phase and disordered γ ($A1$) phase. In the present study, three types of models are used to represent the Gibbs energy functions of these phases: (i) the substitutional solution model for liquid; (ii) the compound-energy formalism (CEF) for the β ($B2$) phase; and (iii) the CSA model for the face-centered cubic (fcc)-based phases with different degrees of order ($A1$, $L1_0$ and $L1_2$). The model for each individual phase is discussed in the following.

2.1. Substitutional solution phases

The liquid phase was modeled as a substitutional solution phase and its Gibbs energy is described by the following formalism:

$$G_m^{\varphi} = {}^{ref}G_m^{\varphi} + {}^{id}G_m^{\varphi} + {}^{ex}G_m^{\varphi} \tag{1}$$

The term ${}^{ref}G_m^{\varphi}$ defines the reference state, which is represented as:

$${}^{ref}G_m^{\varphi} = \sum_i x_i \cdot {}^{o}G_i^{\varphi} \tag{2}$$

where x_i is the mole fraction of element i (i = Ni, Al, Cr or Ir), and ${}^{o}G_i^{\varphi}$ the molar Gibbs energy of the element i with the structure φ.

The term ${}^{id}G_m^{\varphi}$ is related to the molar configurational entropy, which is described as:

$${}^{id}G_m^{\varphi} = RT\sum_i x_i \ln x_i \tag{3}$$

The last term ${}^{ex}G_m^{\varphi}$ is the excess Gibbs energy, which can be described as:

$${}^{ex}G_m^{\varphi} = \sum_{i,j} x_i x_j L_{i,j}^{\varphi} + \sum_{i,j,k} x_i x_j x_k L_{i,j,k}^{\varphi} \tag{4}$$

where i, j, k represent the four components Ni, Al, Cr, Ir. The first term on the right-hand side is the excess Gibbs energy contribution from the six constituent binary phases: Ni–Al, Ni–Cr, Ni–Ir, Al–Cr, Al–Ir, and Cr–Ir. The second term on the right-hand side is the excess Gibbs energy contribution from the four constituent ternary phases: Ni–Al–Cr, Ni–Al–Ir, Ni–Cr–Ir and Al–Cr–Ir. $L_{i,j}^{\varphi}$ represents the interaction parameters in the binary systems, which can be described by the Redlich–Kister polynomial [13]; while $L_{i,j,k}^{\varphi}$ are the ternary interaction parameters in the ternary systems, which can be described as [14]:

$$L_{i,j,k}^{\varphi} = v_i L_i^{\varphi} + v_j L_j^{\varphi} + v_k L_k^{\varphi} \tag{5}$$

where $v_i = x_i - \frac{1-x_i-x_j-x_k}{3}$, $v_j = x_j - \frac{1-x_i-x_j-x_k}{3}$ and $v_k = x_k - \frac{1-x_i-x_j-x_k}{3}$, and L_i^{φ}, L_j^{φ}, L_k^{φ} represent the ternary interaction parameters.

2.2. Compound energy formalism

The β ($B2$) phase is an ordered body-centered cubic (bcc) phase with the CsCl-type structure, which has been found to be stable up to very high temperatures in many alloy systems, such as Al–Ni and Al–Co. The formula $(Al, Cr, Ir, Ni)_1(Cr, Ir, Ni, Va)_1$ is employed to describe the β phase and the Gibbs energy of the β phase can be expressed by using the CEF [15,16] as to be discussed briefly below.

The Gibbs energy per mole of formula unit, i.e. $2 - y''_{Va}$ mole of atoms, is expressed as follows:

$$G_m = \sum_i \sum_j y'_i y''_j G^{B2}_{i:j} + RT\left(\sum_i y'_i \ln y'_i + \sum_j y''_j \ln y''_j\right) + \sum_i \sum_k \sum_j y'_i y'_k y''_j L^{B2}_{i,k:j} + \sum_i \sum_j \sum_l y'_i y''_j y''_l L^{B2}_{i:j,l} \tag{6}$$

where i, j, k, l represent species including Va, and y'_i denotes the site fraction of i on the first sublattice, and y''_j denotes the site fraction of j on the second sublattice. In this Eq. (6), $G^{B2}_{i:j}$, which corresponds to the formation energy of β–ij structure in each i–j binary system, is the so-called end member. The value of an end member can be determined experimentally if β–ij is a stable phase; it can be obtained by ab intio calculation or simply treated as a model parameter if β–ij is not a stable phase.

2.3. fcc Phase

The cluster/site approximation (CSA), first introduced by Fowler [17] for treating atom/molecule equilibria and later adopted and improved for solid alloys [18–24], was employed to describe the thermodynamics of the fcc-based phases (ordered $L1_2$ phase γ' and disordered $A1$ phase γ) in the Ni–Al–Cr–Ir system. The CSA has been successfully used to model the fcc-based phases for a number of Ni-based alloy systems, such as Ni–Al [7], Ni–Al–Cr [8] and Ni–Al–Ir [9]. In the CSA model, the configurational entropy involves only the cluster entropy S_n and single-site entropy S_1. The entropy per site, S_{site} can be written as:

$$S_{site} = \zeta S_n - (n\zeta - 1)S_1 \tag{7}$$

where ζ is the number of energetically non-interfering clusters per site. In the nearest-neighbor pairwise approximation, as was used by Yang and Li [18–21], $\zeta = z/2p$,

where z is the nearest-neighbor coordination number and p the number of nearest-neighbor pairs in the cluster of size n. In the current CSA model, the ζ is used as an adjustable parameter with a value close to $z/2p$. $\zeta = 1.35$ is used in this study instead of the ideal value of 1.0 in the fcc lattice. Although the adjustment in the mixing entropy caused by this modification is quite small, it is critical in making the CSA model applicable to real alloy systems. The dimensionless cluster and site entropies S_n, S_1 are given by $S_n = -\sum_i Z_i \ln Z_i$ and $S_1 = -\sum_i X_i \ln X_i$, respectively, with Z_i being the cluster probability and X_i the point probability. The molar equilibrium free energy G_m for system with C components is given by [7]:

$$\frac{G_m}{RT} = \zeta\left(\sum_P^{C-1}\sum_{i=1}^{n} y_P^i \mu_P^i - \ln\lambda\right) - (n\zeta - 1)\left(\sum_P^{C}\sum_{i=1}^{n} f^i y_P^i \ln y_P^i\right) \quad (8)$$

where f^i is the fraction of sublattice i, and y_P^i is the sublattice mole fraction of component P on sublattice i. The μ_P^i are Lagrangian multipliers arising from the mass balance constraints and are related to the chemical potentials of the species on the sublattice i. The cluster partition function, λ, is expressed in terms of the cluster energies ε_j and the μ_P^i as:

$$\lambda = \sum_{j=1}^{C^n} \exp\left[\left(\sum_P^{C-1}\sum_{i=1}^{n} \mu_P^i\right)_j - \varepsilon_j\right] \quad (9)$$

where ε_j represents the cluster energy of the cluster j.

One challenge of applying computational thermodynamics to real alloys is the need to describe each phase in the system using a suitable thermodynamic model according to its physical nature. Even though the CALPHAD approach has been used in multicomponent commercial alloys with some success, its predictive capability is sometimes limited due to the use of oversimplified models. For example, ordered intermetallic phases are generally described by sublattice-type models, such as the CEF. In this type of model, the entropy of a phase is calculated by point approximation without considering the contribution of short-range order (SRO). Therefore, it cannot be used to describe phases that exhibit order/disorder transformation, which is a common phenomenon in many metal alloy systems. This is particularly true for Ni-based superalloys, for which the strengthening γ' precipitate phase has an ordered fcc structure ($L1_2$) and the matrix γ phase has a disordered fcc structure ($A1$). It is therefore critically important to use a physically sound model to describe the order/disorder transition between the γ and γ' phases in Ni-based superalloys. The CSA model, which takes both long-range order (LRO) and SRO into consideration, is superior to the traditional Bragg–Williams type of models, and at the same time possesses a computational advantage over the cluster variation method. It is therefore selected in this study to describe the fcc phase in both states, i.e. disordered $A1$ and ordered $L1_2$. On the other hand, it should be pointed out that the CSA model was not adopted for bcc phases in the current work due to the difficulty in cluster selection. Neither a common tetrahedral cluster without considering the second nearest neighbor bonds, nor a bigger cluster considering both nearest neighbor and second nearest neighbor bonds, gives satisfactory results for the bcc lattice. Therefore, as an initial effort to develop a multicomponent thermodynamic database for industrial applications, we chose to adopt the CSA model only for the fcc-based phases.

3. Experimental investigation

Cr is used in commercial Ni-based superalloys at different levels for different purposes. In this study, alloys with 3 at.% Cr were chosen for experimental investigation to validate and improve the preliminary thermodynamic description of Ni–Al–Cr–Ir. This description can then be used to understand the phase equilibria and related properties of Ni–Al–Cr–Ir alloys with low Cr content. This database needs further validation and improvement for alloys with higher Cr contents.

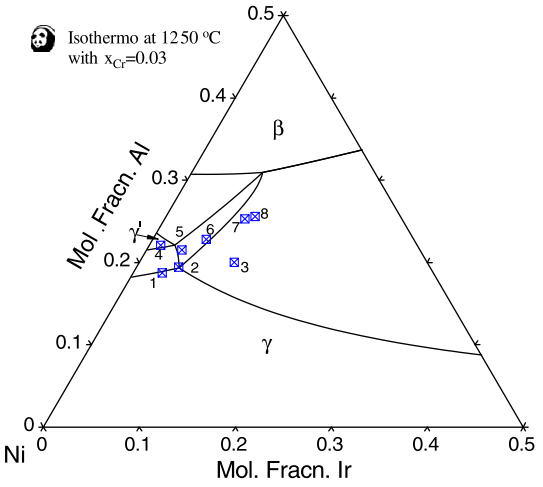

Fig. 1. Calculated isothermal section of the Ni–Al–Cr–Ir system at 1250 °C in the Ni-rich region with $x_{Cr} = 0.03$ using the preliminary description and the selected alloys.

Table 1
Overall compositions of selected alloys in this study.

Alloy no.	Concentration (at.%)			
	Al	Cr	Ir	Ni
1	18.89	3.09	2.19	Bal.
2	19.40	3.08	4.70	Bal.
3	19.98	3.10	9.87	Bal.
4	21.94	2.93	1.03	Bal.
5	22.48	3.07	3.66	Bal.
6	22.77	3.11	5.56	Bal.
7	25.26	3.05	8.34	Bal.
8	25.55	2.99	9.25	Bal.

As mentioned previously, a preliminary quaternary Ni–Al–Cr–Ir thermodynamic description was obtained via extrapolation from those of the constituent lower-order systems. The isothermal section with 3 at.% Cr was calculated at 1250 °C using this preliminary description (as shown in Fig. 1), and eight key alloys were then selected based on this isothermal section for further experimental investigation. These alloys are located either in different phase regions or on the phase boundaries: alloy 1 at the $\gamma/\gamma + \gamma'$ phase boundary, alloy 2 on the corner of the $\gamma + \gamma' + \beta$ tie-triangle, alloy 3 in the $\gamma + \beta$ two-phase region, etc. Thus the most important phase-equilibrium information can be obtained through experimental study of these alloys. Table 1 lists the overall compositions of the selected alloys in this study. All compositions in this paper are in atomic percent, unless otherwise stated.

Al–Ir binary alloys prepared by AFSOR were used as master alloys for alloy preparation in this study. The starting materials used for the master alloys were commercially pure Al with a purity of 99.999% or higher and Ir powder purchased from Engelhard and Carr with a purity of 99.9%. The gross weight for each Al–Ir alloy is about 30 g. The alloys were fabricated by arc-melting under high-purity (99.998%) argon, with titanium as an oxygen-getter. Each alloy button was inverted and remelted at least five times to ensure homogeneity. The

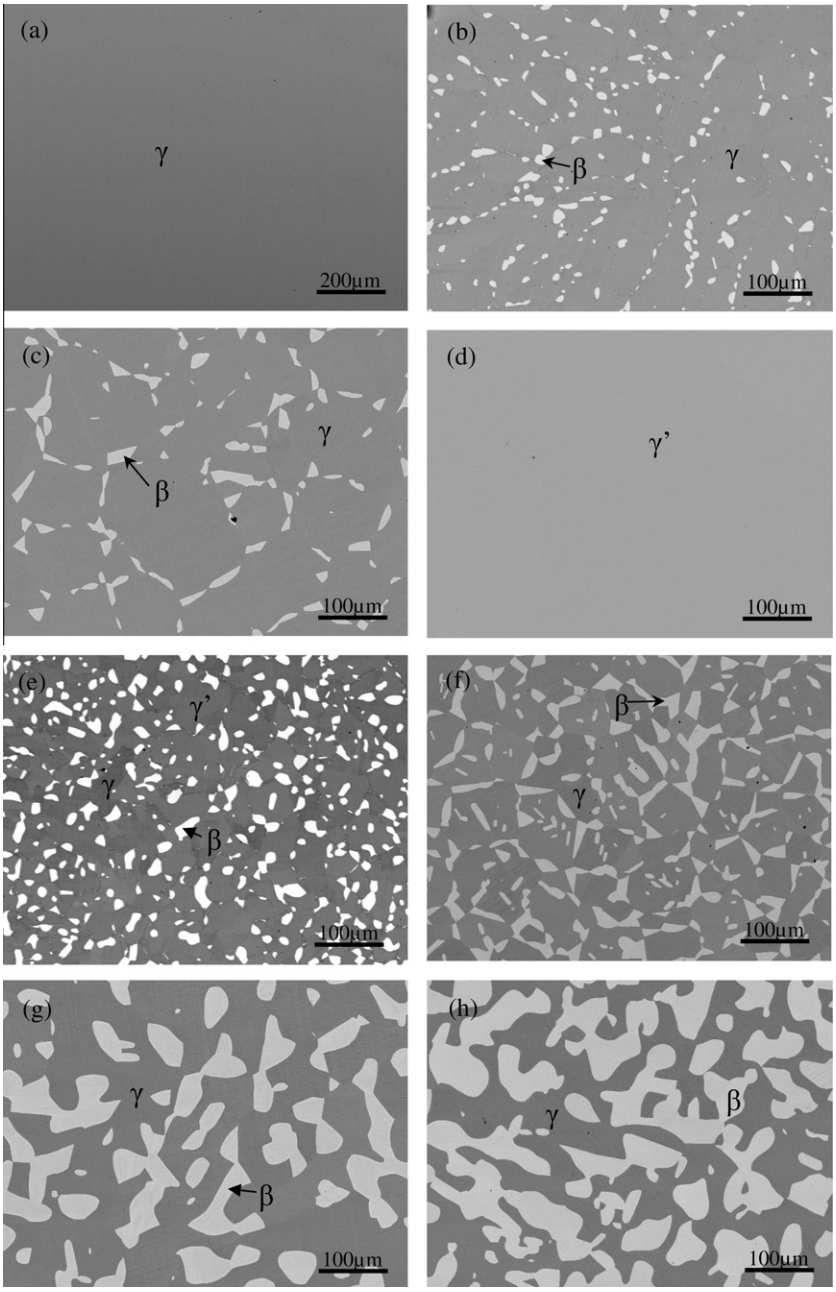

Fig. 2. BSE images of the alloys annealed at 1250 °C for 30 days: (a) alloy 1; (b) alloy 2; (c) alloy 3; (d) alloy 4; (e) alloy 5; (f) alloy 6; (g) alloy 7; (h) alloy 8.

Table 2
Comparison of the calculated and EPMA measured phase compositions of the Ni–Al–Cr–Ir system in equilibrium at 1250 °C in the Ni-rich region.

Alloy	Phase	Calculation (at.%)				Experimentation (at.%)			
		Al	Cr	Ir	Ni	Al	Cr	Ir	Ni
#2	γ	18.67	3.18	4.01	Bal.	17.95	4.17	4.99	Bal.
	β	30.85	1.43	10.46	Bal.	30.93	1.83	11.36	Bal.
#3	γ	16.51	3.59	7.56	Bal.	17.47	4.11	7.82	Bal.
	β	33.36	1.21	18.76	Bal.	31.03	1.85	17.16	Bal.
#5	γ	19.01	4.07	3.08	Bal.	19.63	3.04	2.94	Bal.
	γ'	22.28	2.44	1.82	Bal.	21.35	3.01	2.14	Bal.
	β	30.46	1.96	8.14	Bal.	31.46	2.15	6.53	Bal.
#6	γ	18.78	3.67	3.61	Bal.	18.71	3.38	4.05	Bal.
	β	30.68	1.69	9.44	Bal.	30.10	1.67	8.13	Bal.
#7	γ	17.94	4.47	4.97	Bal.	17.89	3.34	5.34	Bal.
	β	31.31	1.90	11.49	Bal.	30.01	1.66	10.55	Bal.
#8	γ	17.66	4.47	4.96	Bal.	18.44	4.61	4.44	Bal.
	β	31.59	1.85	12.53	Bal.	30.07	2.12	12.43	Bal.

overall compositions of the Al–Ir binary alloys were determined by electron probe microanalysis (EPMA) [10]. In this study, one single-phase Al–Ir binary alloy (Ir–49.88Al) was used as the master alloy. High-purity elements (99.995% Ni slugs, 99.999% Al slugs and 99.995% Cr pieces) were then used as additions to the master alloys in order to obtain the selected overall compositions. The mixed materials were arc-melted into small buttons in a high-purity argon atmosphere. The gross weight for each sample is about 1 g, and the weight loss during preparation is less than 0.3 wt.%. Each sample was then cut into two pieces using a diamond wheel cutter: one piece was wrapped in tantalum foil for isothermal annealing at 1250 °C for one month in a high-purity argon atmosphere; the other was used for as-cast microstructural analysis. Note that the annealing temperature at 1250 °C is close to the operating temperatures (about 1200 °C) of Ni-based superalloys with the addition of Pt, Ir or Rh. Thus phase-equilibrium information at around this temperature is of particular interest.

Both the as-cast and annealed samples were carefully ground to obtain scratch-free surfaces. The microstructure of each sample was examined by scanning electron microscopy (SEM) using a JEOL6100 in backscattered electron (BSE) imaging mode. The phase compositions were determined by EPMA performed with a CAMECA SX51 electron probe.

4. Results and discussions

The effect of Cr on the phase stability of the Ni–Al–Ir system will be discussed from the following three aspects in terms of both calculation and experiment: (1) solid-state phase equilibria of the Ni–Al–Cr–Ir system at 1250 °C; (2) liquid–solid phase equilibria of the Ni–Al–Cr–Ir alloys described by two-dimensional (2-D) sectional liquidus projections; (3) isoplethal sections of Ni_3Al–Ir_3Al with $x_{Cr} = 0.03$ and Ni_3Al–Cr_3Al with $x_{Ir} = 0.03$.

4.1. Solid-state phase equilibria of the Ni–Al–Cr–Ir system at 1250 °C

The microstructure images of the eight selected Ni–Al–Cr–Ir quaternary alloys annealed at 1250 °C for 30 days were determined by BSE as shown in Fig. 2. Alloy 1 is found to be a single-phase alloy as shown in Fig. 2a. EPMA and SEM/EDS (energy-dispersive spectroscopy) analyses indicate that this phase is γ phase. The microstructure of alloy 2 as shown in Fig. 2b reveals the coexistence of two distinct phases. EPMA measurements suggest that these two phases are γ (gray phase) and β (bright phase). The larger amount of the γ phase implies that the overall composition of this alloy is located very close to the $\gamma/\gamma+\beta$ boundary. The microstructure of alloy 3 shown in Fig. 2c, with γ and β phases coexisting, is similar to that of alloy 2. Alloy 4 was also found to be a single phase as

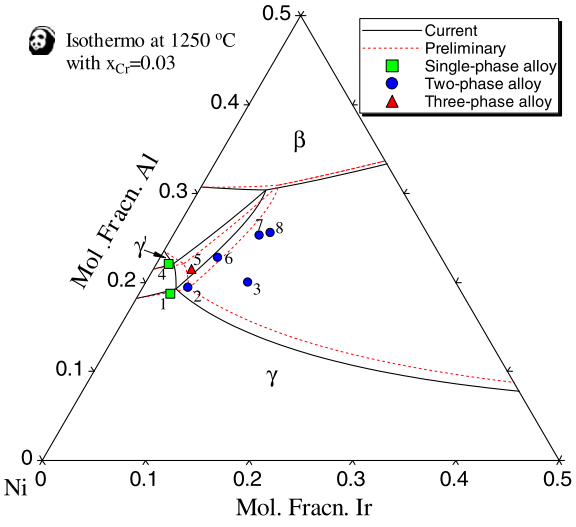

Fig. 3. Comparison between the isothermal sections using the preliminary and the current descriptions at 1250 °C of the Ni–Al–Cr–Ir system in the Ni-rich region.

shown in Fig. 2d. This phase was determined by EPMA to be the γ' phase. The microstructure of alloy 5 in Fig. 2e shows that three phases coexisted. EPMA and SEM/EDS analyses indicate that the dark phase is γ, the gray phase is γ' and the bright phase is β. The microstructures of alloys 6–8 shown in Fig. 2f–h are similar to each other and clearly show a two-phase mixture of γ (gray phase) and β (bright phase) at this temperature. The large volume fraction of β phase in alloy 8 indicates that its overall composition is closer to the $\gamma + \beta/\beta$ than those of alloys 6 and 7. The EPMA measured compositions of phases in equilibrium for these eight alloys are listed in Table 2.

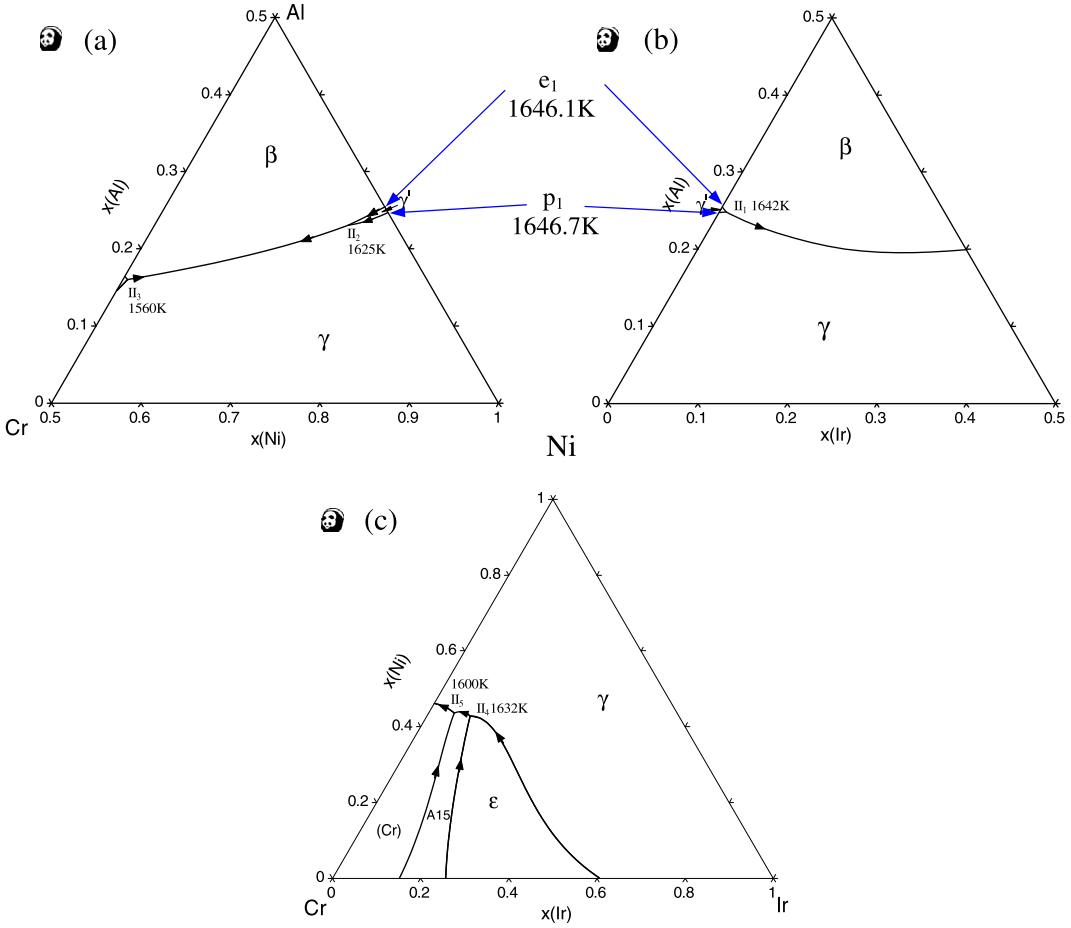

Fig. 4. The calculated liquidus projections of three Ni constituent ternaries, Ni–Al–Cr, Ni–Al–Ir and Ni–Cr–Ir, of the quaternary Ni–Al–Cr–Ir system.

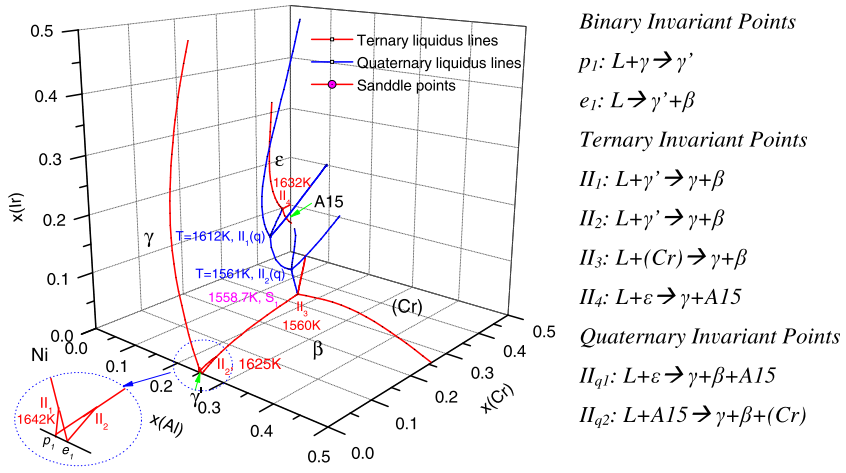

Fig. 5. Calculated liquidus projection of the Ni–Al–Cr–Ir quaternary system in the Ni-rich region. The red line denotes the univariant lines in the the constituent ternaries; the blue line denotes the univariant lines in the quaternary. The reactions denoted by p_i, e_i and Π_i are shown in the legend.

Table 3
Calculated phase compositions of the Ni–Al–Cr–Ir system at invariant temperatures in the Ni-rich region.

Invariants	Reaction	T (°C)	Phase	Composition, mole fraction			
				x(Al)	x(Cr)	x(Ir)	x(Ni)
II_1(q)	$L + \varepsilon \rightarrow \gamma + \beta + A15$	1339	L	0.1202	0.3046	0.1102	Bal.
			ε	5.9E−5	0.6361	0.3387	Bal.
			γ	0.0912	0.2806	0.1451	Bal.
			β	0.3562	0.0936	0.2568	Bal.
			$A15$	1.0E−6	0.7339	0.2661	Bal.
II_2(q)	$L + A15 \rightarrow \gamma + \beta + (Cr)$	1288	L	0.1327	0.3485	0.0375	Bal.
			γ	0.1034	0.3573	0.0287	Bal.
			β	0.3276	0.1248	0.0924	Bal.
			$A15$	1.0E−6	0.7864	0.2136	Bal.
			(Cr)	0.0049	0.7995	0.0848	Bal.

As mentioned in the Introduction, the preliminary thermodynamic description of the Ni–Al–Cr–Ir quaternary system was built upon four unary systems, six binary systems (Ni–Al [7], Ni–Cr [8], Ni–Ir [9], Al–Cr [8], Al–Ir [10] and Cr–Ir [11]), and four ternary systems (Ni–Al–Cr [8], Ni–Al–Ir [9], Ni–Cr–Ir and Al–Cr–Ir). The descriptions of the Ni–Cr–Ir and Al–Cr–Ir systems are obtained from those of the constituent binary phases by extrapolation due to the lack of experimental data. They are therefore less accurate. By comparing the calculated isothermal section Ni–Al–Ir–0.03Cr at 1250 °C using the preliminary description of the quaternary system with the experimental data obtained in this study, some discrepancies were observed as shown in Fig. 1. From the preliminary description, alloy 1 is at the $\gamma/\gamma + \gamma'$ phase boundary, alloy 2 and alloy 6 are in the $\gamma + \gamma' + \beta$ three-phase triangle, while experimental data show that alloy 1 is single γ phase, and both alloy 2 and alloy 6 are in the $\gamma + \beta$ two-phase field. According to the EPMA measurements and the microstructure data obtained in this study, ternary interaction parameters are optimized for the fcc phase in the Ni–Cr–Ir ternary system. Thus an improved thermodynamic description for the Ni–Al–Cr–Ir system was obtained via the CALPHAD approach.

As shown in Fig. 3, comparison is made between the calculated partial isothermal sections at 1250 °C using the preliminary description and the improved description as well as the experimental results obtained in this study. The red dashed lines are the phase boundaries calculated using the preliminary description, and the solid lines show the calculated phase boundaries using the improved description. The square symbols represent the single-phase alloys. The solid circle symbols indicate two-phase alloys and the triangle symbol shows the overall composition of the three-phase alloy. Fig. 3 shows that the calculation using the improved description can accurately describe the experimental data of this study. In addition, Table 2 compares the calculated compositions of phases in equilibrium with the EPMA measurements. It shows that the calculations agree well with the experimental measurements and the discrepancies are within ~2 at.%. Note that the EPMA measured phase compositions were not used to optimize the thermodynamic parameters of the current description; they are simply used to validate the improved thermodynamic description we developed for the Ni–Al–Cr–Ir quaternary system in the Ni-rich region.

4.2. Liquid–solid phase equilibria of the Ni–Al–Cr–Ir alloys in the Ni-rich region

In order to understand solidification of an alloy and its solidified microstructure, which governs its properties and ultimately its performance in service, phase diagrams are usually used to estimate its phase formation sequences during nonequilibrium solidification in a simple system, such as binary or ternary system. However, the task becomes much more challenging when we carry out such an analysis for a quaternary system, not to mention even higher-order systems. Yet, most real alloys, such as the Ni-based superalloys, consist of at least four component elements. Taking advantage of the commercial software Pandat [25,26] for calculating multicomponent phase diagrams, prediction of phase formation sequences during nonequilibrium solidification becomes possible for multicomponent system. In this section, solidification simulations for the Ni–Al–Cr–

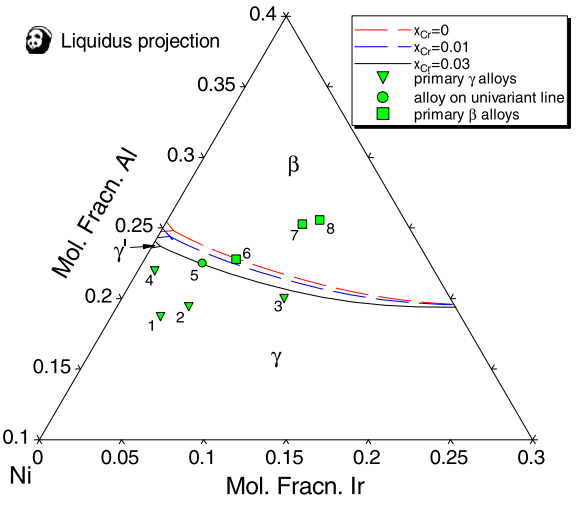

Fig. 6. Calculated 2-D sectional liquidus projection of the Ni–Al–Cr–Ir system in the Ni-rich region with different Cr concentrations as well as the overall compositions of the selected alloys.

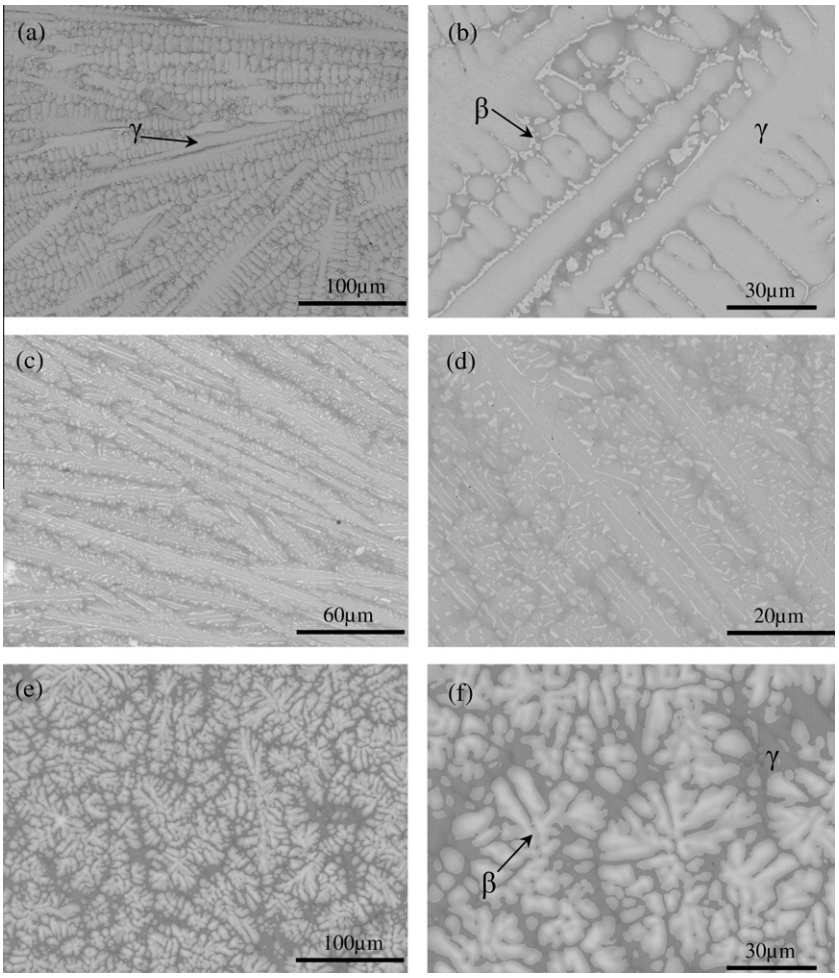

Fig. 7. BSE images show the as-cast microstructures of selected alloys in this study. The bright phase is β and the gray phase is γ: (a and b) alloy #2 (Ni–19.40Al–3.08Cr–4.70Ir); (c and d) alloy #5 (Ni–22.48Al–3.07Cr–3.66Ir); (e and f) alloy #7 (Ni–25.26Al–3.05Cr–8.34Ir).

Ir alloys selected in this study will be carried out and the calculated results compared with those observed in the as-cast structure.

Conventionally, the liquidus surface in the ternary system is projected along the temperature direction onto the 2-D compositional plane as the liquidus projection. From the liquidus projection, the primary phase solidified from the liquid and the subsequent solidification sequence are indicated. However, the task becomes much more challenging when such an analysis is carried out for a quaternary or even higher-order system. In the following, the thermodynamically calculated liquidus projection for the Ni–Al–Cr–Ir system in the Ni-rich corner is used to visualize the solidification paths of the quaternary Ni–Al–Cr–Ir alloys.

Fig. 4 shows the calculated liquidus projections for the three ternaries that involve Ni: Ni–Al–Ir, Ni–Al–Cr and Ni–Cr–Ir of the Ni–Al–Cr–Ir quaternary system. The compositions are given as mole fraction, denoted as x(Ni), x(Al), x(Cr) and x(Ir), respectively. The symbols γ, γ', β, ε, $A15$ and (Cr) denote the disordered fcc ($A1$) phase, the ordered fcc ($L1_2$), the ordered bcc ($B2$), the ordered hexagonal close packed (hcp), the Cr_3Ir intermetallic phase, and the disordered bcc ($A1$), respectively. The two invariant reactions in the Ni–Al binary are denoted as p_1: $L + \gamma = \gamma'$ (1646.7 K) and e_1: $L = \gamma' + \beta$ (1646.1 K). The five type II ternary invariant reactions are II_1: $L + \gamma' = \gamma + \beta$ (Ni–Al–Ir, 1642 K), II_2: $L + \gamma' = \gamma + \beta$ (Ni–Al–Cr, 1625 K), II_3: $L + (Cr) = \gamma + \beta$ (Ni–Al–Cr, 1560 K), II_4: $L + \varepsilon = \gamma + A15$ (Ni–Cr–Ir, 1632 K) and II_5: $L + A15 = \gamma + (Cr)$ (Ni–Cr–Ir, 1600 K). For the quaternary system, the liquidus surface is projected along the temperature direction onto the 3-D compositional space to form the liquidus projection. Fig. 5 shows the calculated 3-D liquidus projection of the Ni–Al–Cr–Ir quaternary system in the Ni corner with x_{Al}, x_{Cr} and x_{Ir} less than 0.5. A simple explanation of how to read the quaternary liquidus projection is given below and readers are referred to the Ref. [27] for more detail. As shown in Fig. 5, the compositions of the liquid for the univariant three-phase equilibria $L + \text{solid}_1 + \text{solid}_2$ in the ternary and four-phase equilibria $L + \text{solid}_1 + \text{solid}_2 + \text{solid}_3$ in the quaternary are indicated as red lines and blue[1] lines, respectively. There are a total of

[1] For interpretation of color in Figs. 3, 5 and 6, the reader is referred to the web version of this article.

two five-phase invariant reactions as denoted by $II_1(q)$ ($L+\varepsilon \rightarrow \gamma+\beta+A15$) and $II_2(q)$ ($L+A15 \rightarrow \gamma+\beta+(Cr)$) in the Ni-rich region, with the symbol (q) indicating that they are for the quaternary system. The calculated compositions of the phases and temperatures at the invariant equilibria are given in Table 3. The primary phase solidified from the Ni–Al–Cr–Ir liquid in the Ni corner can be seen in overview in Fig. 5 given different concentrations of Al, Cr or Ir. In the commercial Ni-based superalloys, the Al concentration is less than 25 at.% and only a few per cent Ir is needed. One can tell from Fig. 5 that the primary phases solidified from the liquid can be either γ or β if the Cr concentration is less than 25 at.%. The γ' primary phase is also possible within the specific Al concentration region (~20 at.%). The liquidus surfaces in the quaternary liquidus projection are composed of 3-D volumes in the space and are difficult to visualize. In order to obtain a better view of the multicomponent liquidus surface, the 2-D sectional liquidus projection can be calculated by Pandat [28] for a fixed composition of the fourth element. Even though some information is lost when the 3-D plot is projected to 2-D, the 2-D sectional liquidus projections are easy to visualize and very useful for understanding the solidification sequence. Three 2-D sectional liquidus projections with different Cr concentrations are calculated using the Ni–Al–Cr–Ir database developed in this study as shown in Fig. 6. The red dotted lines show the univariant liquidus in the Ni–Al–Ir ternary system without Cr. The blue dashed lines and the black solid lines indicate the univariant liquidus in the Ni–Al–Cr–Ir quaternary system with $x(Cr) = 0.01$ and 0.03, respectively. Fig. 6 shows that the β primary phase field expands with the increasing of Cr concentration, which indicates that the addition of Cr increases the stability of the β phase in the Ni-based Ni–Al–Cr–Ir alloys.

As discussed in Section 2, as-cast microstructural analysis was also carried out for the selected alloys in this study, and the as-cast microstructures are also used to validate the calculations. As indicated in Fig. 6, the primary phases solidified from the liquid of alloys 1–4 are γ phase, and the primary phases of alloys 6–8 are all β phase. Since alloy 5 is located almost on the univariant line, the γ and β phases will form simultaneously. Fig. 7 shows the BSE images of the typical as-cast microstructure of alloys 2, 5 and 7. The as-cast microstructure of alloy 2 is shown in Fig. 7a and b. Fig. 7a indicates the existence of one major phase in dendritic morphology, which is identified by SEM/EDS as the primary γ phase. The higher-magnification BSE image of the same alloy 2 is shown in Fig. 7b. It reveals a eutectic-like structure (gray phase + bright phase) in the interdendritic region. The bright phase is identified as the β phase and the gray phase as the γ phase. The small contrast difference between the primary and the interdendritic γ phase is probably due to macrosegregation during solidification. The as-cast microstructure of alloy 5 (Fig. 7c), which shows a majority of eutectic-like structure (gray phase + bright phase) and small amount of dark region between the eutectic-like dendrites, reveals the fact that the primary solidification is a two-phase eutectic mixture. Fig. 7d shows higher-magnification BSE images of the as-cast microstructure of alloy 5. The SEM/EDS results indicate that the dark phase and gray phase have the same chemistry and they are both identified as the γ phase. The contrast of this phase in the two regions is again due to macrosegregation. The bright phase is identified to be the

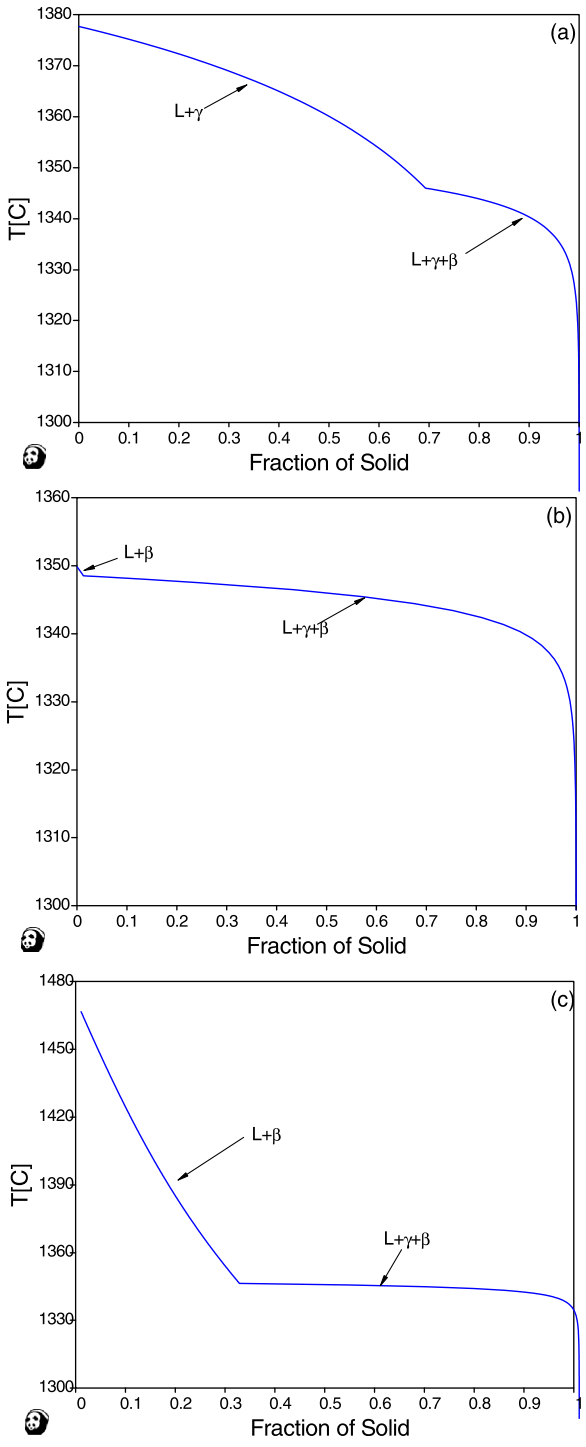

Fig. 8. Calculated solidification paths using the Scheil model: (a) alloy 2; (b) alloy 5; (c) alloy 7.

β phase. The as-cast microstructure of alloy 7 shown in Fig. 7e clearly reveals the existence of one dominant phase with bright contrast in the dark matrix. The SEM/EDS analysis indicates that the bright phase is β. The dendritic morphology of the β phase in the as-cast microstructure suggests that it is the primary phase of solidification. However, Fig. 7f, which is the higher-resolution as-cast microstructure of alloy 7, indicates the existence of a small amount of eutectic-like structure in the interdendritic region. This will be discussed in the next paragraph together with solidification path simulation.

In addition to the information of the primary solidified phase as obtained from the 2-D sectional liquidus projection (Fig. 6), the solidification paths of alloys 2, 5 and 7 are simulated using the Scheil model [29], which is based on the assumptions that local equilibrium prevails at the liquid–solid interfaces, no diffusion takes place in the solids and infinitely fast diffusion occurs in the liquid. The simulated solidification paths of alloys 2, 5 and 7 are shown in Fig. 8. As seen from Fig. 8a, the primary solidified phase of alloy 2 is γ with a fraction of about 70%. The phase-forming sequence of alloy 2 is: $L \rightarrow L+\gamma \rightarrow L+\gamma+\beta \rightarrow \gamma+\beta$, which agrees well with the experimental observation as shown in Fig. 7a and b. The solidification path of alloy 5 as shown in Fig. 8b, which indicates that the primary phase β is only ~1%, and the majority fraction of solid is $\gamma+\beta$ eutectic-like mixture, agrees with the experimentally observed as-cast microstructure shown in Fig. 7c and d. The simulated solidification path of alloy 7 is: $L \rightarrow L+\beta \rightarrow L+\gamma+\beta \rightarrow \gamma+\beta$ as shown in Fig. 8c. The β phase is the primary phase solidified from the liquid, followed by the $\gamma+\beta$ eutectic-like structure. However, the temperature gradient during the solidification of $L \rightarrow \gamma+\beta$ is very small, which leads to coarsening of the phases involved in the eutectic-like structure. This explains why a few gray blocks (β phase) are embedded in the dark matrix (γ phase) in the interdendritic region as shown in Fig. 7f.

As demonstrated in Sections 4.1 and 4.2, the thermodynamic database developed in this work for the Ni–Al–Cr–Ir system can successfully describe both the phase equilibria at 1250 °C and the solidification behavior of the Ni–Al–Cr–Ir alloys in the Ni-rich region. We may thus conclude that we can use it to understand the phase relationships in this quaternary and understand the effect of Cr on the phase stability as will be discussed in the next section.

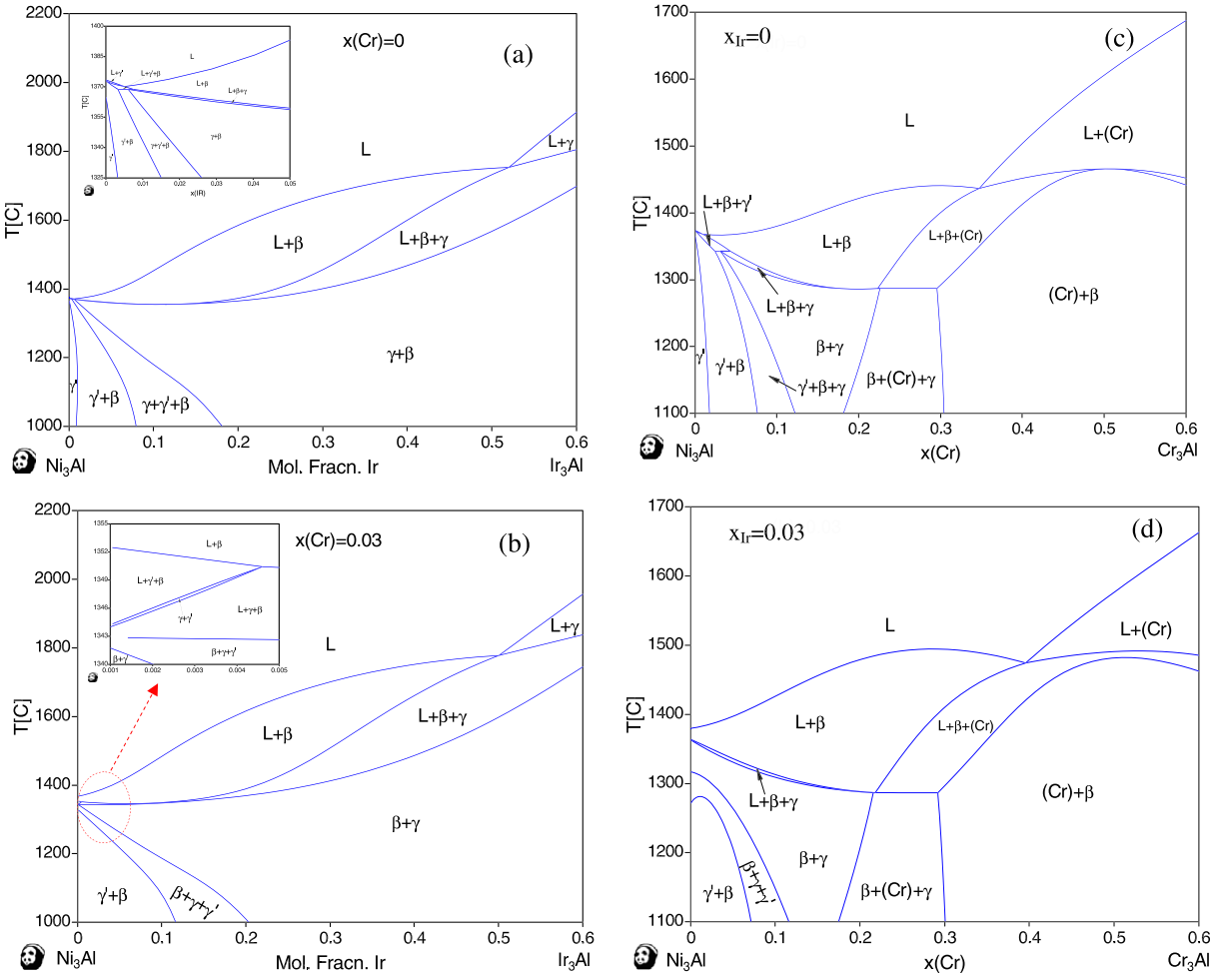

Fig. 9. Calculated isopleths: (a) Ni_3Al to Ir_3Al with $x_{Cr} = 0.0$; (b) Ni_3Al to Ir_3Al with $x_{Ir} = 0.03$; (c) Ni_3Al to Cr_3Al with $x_{Ir} = 0.0$; (d) Ni_3Al to Cr_3Al with $x_{Ir} = 0.03$.

4.3. Isoplethal phase diagrams

An isopleth is a temperature–concentration phase diagram of a ternary or higher-order system, and is a vertical two-dimensional section with temperature as one axis, and composition as the other. In this study, four isopleths (shown in Fig. 9) are calculated in order to investigate the effect of Cr addition on the Ni–Al–Cr–Ir quaternary alloys in the Ni-rich region. Fig. 9a and b show the calculated isopleths of Ni_3Al–Ir_3Al with fixed Cr concentration at $x_{Cr} = 0$ and $x_{Cr} = 0.03$, respectively. Fig. 9a clearly demonstrates the phase stability change when Ir is used to substitute Ni along Ni_3Al–Ir_3Al section in the temperature range from 1000 to 2200 °C. At the pure Ni_3Al side, γ' is the only stable phase at low temperature, while β and γ become stable when Ni is replaced by Ir. Fig. 9b shows the effect of Cr on the phase relationship of the Ni_3Al–Ir_3Al section. It can be seen that 3 at.% Cr completely eliminates the single γ' phase field even when 0% Ir is used. The $\beta + \gamma'$ two-phase field becomes wider when 3 at.% Cr is used. In order to further investigate the effect of Cr addition on the Ni–Al–Cr–Ir alloys, two more isopleths (shown in Fig. 9c and d) of Ni_3Al–Cr_3Al with $x_{Ir} = 0$ and $x_{Ir} = 0.03$ are calculated, respectively. As revealed by Fig. 9c, addition of Cr leads to the formation of β and (Cr). Fig. 9d illustrates the effect of 3 at.% Ir on the phase relationship along the Ni_3Al–Cr_3Al section. Again, 3 at.% Ir eliminates the single γ' phase region at the Ni_3Al side, while 3 at.% Ir does not have any significant effect on the phase relation at the Cr_3Al-rich side.

5. Summary

Calculation of multicomponent phase diagrams is an important tool for alloy development and process optimization. The thermodynamic description developed in this study for the Ni–Al–Cr–Ir system using computational/experimental methods is critically important in the development of a multicomponent thermodynamic database for Ni alloys containing Ir. The EPMA measured compositions of phases in equilibrium at 1250 °C are consistent with the calculations. The calculated 2-D sectional liquidus projection and simulated solidification paths agree well with the as-cast microstructural analysis. The calculated isopleths are believed to offer a better understanding of the resulting microstructures in Ni–Al–Cr–Ir alloys.

References

[1] Caldwell EC, Fela FJ, Fucks GE. JOM 2004(September):44.
[2] Gleeson B, Wang W, Hayashi S, Sordelet D. Mater Sci Forum 2004;461–464:213.
[3] Gleeson B, Sordelet DJ. US Pat Appl Publ 2006; 22 pp.
[4] Van Sluytman JS, Suzuki A, Bolcavage A, Helmink RC, Ballard DL, Pollock TM. Superalloys 2008:499–508.
[5] Cao HB, Zhu J, Zhang C, Wu KS, Saddock ND, Jones JW, et al. Int J Mater Res 2006;97(4):422.
[6] Zhang C, Zhu J, Yang Y, Cao HB, Zhang F, Cao WS, et al. Intermetallics 2008;16(2):139.
[7] Zhang F, Chang YA, Du Y, Chen S-L, Oates WA. Acta Mater 2003;51:207.
[8] Cao W, Zhu J, Yang Y, Zhang F, Chen S-L, Oates WA, et al. Acta Mater 2005;53:4189.
[9] Zhang C, Zhu J, Bengtson A, Morgan D, Zhang F, Cao W-S, et al. Acta Mater 2008;56(11):2576.
[10] Zhang C, Zhu J, Yang Y, Zhang F, Chang YA. Scripta Mater 2008;59(4):403.
[11] Zhang C, Zhu J, Morgan D, Yang Y, Zhang F, Cao W-S, et al. CALPHAD 2009;33(2):420–4.
[12] Chou KC, Chang YA, Bunsenges Ber. Phys Chem 1989;93:735.
[13] Redlich O, Kister A. Ind Eng Chem 1948;40:345.
[14] Lukas HL, Weiss J, Henig E-Th. CALPHAD 1982;6(3):229.
[15] Hillert M, Staffansson LI. Acta Chem Scand 1970;24(10):3618.
[16] Anderson JO, Guillermet AF, Hillert M, Jason B, Sundman B. Acta Matell. 1986;34:437.
[17] Fowler RH. In: Statistical mechanics. Cambridge: Cambridge University Press; 1938. p. 162–4.
[18] Yang CN. J Chem Phys 1945;13:66.
[19] Yang CN, Li Y. Chin J Phys 1947;7:59.
[20] Li Y. J Chem Phys 1949;17:447.
[21] Li Y. Phys Rev 1949;76:972.
[22] Oates WA, Wenzl H. Scripta Mater 1996;35:623.
[23] Oates WA, Zhang F, Chen S-L, Chang YA. Phys Rev B 1999;59:11211 (17).
[24] Cao W, Chang YA, Zhu J, Chen S-L, Oates WA. Acta Mater 2005;53:331.
[25] Pandat 8.0—Phase Diagram Calculation Software for Multi-Component Systems. CompuTherm, Madison, WI; 2008.
[26] Cao W, Chen S-L, Zhang F, Wu K, Yang Y, Chang YA, et al. CALPHAD 2009;33(2):328–42.
[27] Chang YA. Metall Trans B 2006;37B:7.
[28] Chen S-L, Yang Y, Cao W, Bewlay BP, Chou KC, Chang YA. J Phase Equilib Diffus 2008;29(5):390.
[29] De Fontaine D. In: Ehrenreich H, Turubull D, editors. Solid state physics, vol. 47. New York: Academic Press; 1994. p. 33–176.